HHS Public Access

Author manuscript

Free Radic Biol Med. Author manuscript; available in PMC 2021 November 20.

Published in final edited form as:

Free Radic Biol Med. 2020 November 20; 160: 57–66. doi:10.1016/j.freeradbiomed.2020.07.002.

Dynasore Protects Ocular Surface Mucosal Epithelia Subjected to Oxidative Stress by Maintaining UPR and Calcium Homeostasis

Rafael Martinez-Carrasco[1], **Pablo Argüeso**[2], **M. Elizabeth Fini**[1,3,*]

[1]New England Eye Center of Tufts Medical Center, Department of Ophthalmology, Tufts University School of Medicine, Boston, MA

[2]Schepens Eye Research Institute of Massachusetts Eye and Ear, Department of Ophthalmology, Harvard Medical School, Boston, MA

[3]Program in Pharmacology and Drug Development, Tufts Graduate School of Biomedical Sciences, Tufts University, Boston, MA

Abstract

The mucosal epithelia of the ocular surface protect against external threats to the eye. Using a model of human stratified corneal epithelial cells with mucosal differentiation, we previously demonstrated that a small molecule inhibitor of dynamin GTPases, dynasore, prevents damage to cells and their transcellular barriers when subjected to oxidative stress. Investigating mechanisms, we now report the novel finding that dynasore acts by maintaining Ca^{+2} homeostasis, thereby inhibiting the PERK branch of the unfolded protein response (UPR) that promotes cell death. Dynasore was found to protect mitochondria by preventing mitochondrial permeability transition pore opening (mPTP), but, unlike reports using other systems, this was not mediated by dynamin family member DRP1. Necrostatin-1, an inhibitor of RIPK1 and lytic forms of programmed cell death, also inhibited mPTP opening and further protected the plasma membrane barrier. Significantly, necrostatin-1 did not the protect the mucosal barrier. Oxidative stress increased mRNA for *sXBP1*, a marker of the IRE1 branch of the UPR, and *CHOP*, a marker of the PERK branch. It also stimulated phosphorylation of eIF2α, the upstream regulator of *CHOP*, as well as an increase in intracellular Ca^{2+}. Dynasore selectively inhibited the increase in PERK branch markers, and also prevented the increase intracellular Ca^{2+} in response to oxidative stress. The increase in PERK branch markers were also inhibited when cells were treated with the cell

*Corresponding Author: mefini@tuftsmedicalcenter.org.

Author contributions: R.M-C contributed to the study design, collected and analyzed the data, and wrote the first draft of the manuscript. P.A. contributed to the study design and revised the manuscript. M.E.F. supervised the study, contributed to the study design and data analysis, and finalized the manuscript.

Competing interests: M.E.F. serves as MPI on NIH grant R41-EY030811 awarded to MedChem Partners, Lexington, MA with the goal to develop dynasore analogues to treat ocular surface disease. The other authors declare that they have no competing interests.

Data and materials availability: All data needed to evaluate the conclusions in the paper are present in the paper.

permeable Ca^{2+} chelator, BAPTA-AM. To our knowledge, this is the first time that dynasore has been shown to have an effect on the UPR and suggests therapeutic applications.

Graphical Abstract

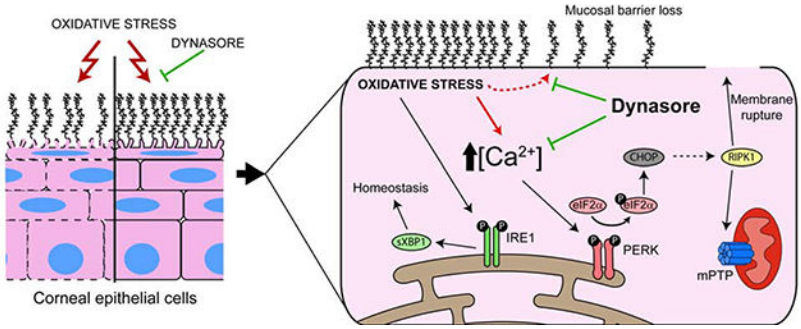

One Sentence Summary

Dynasore protects ocular surface mucosal epithelia subjected to oxidative stress by maintaining calcium homeostasis, thereby inhibiting the PERK branch of the unfolded protein response (UPR) that promotes cell death.

Introduction

The mucosal corneal and conjunctival epithelia of the ocular surface play an essential role as a barrier against external threats to the eye (1). The squamous cells at the apical layer of these epithelia are linked by tight junctions that seal the paracellular space and prevent the passage of toxic substances to the cells and tissues beneath (2). In addition, these cells express mucins on their plasma membrane that, along with galectins, form the sugar-rich glycocalyx responsible for stabilizing the tear film and repelling pathogens and other noxious agents (3–5). Protecting the apical epithelial cells and their glycocalyx against damage is crucial to prevent ocular surface disease and infection.

Dynasore is a cell-permeable small molecule that has been shown to selectively inhibit the GTPase activity of classic dynamins DNM1 and DNM2. It was developed as a tool for the study of classic dynamin-related functions such as receptor-mediated endocytosis and cell migration (6). However, “off-target” effects have been demonstrated that are independent of classic dynamins (7–10). Some of these effects might be attributed to targeting of other members of the dynamin family (11). For example, in a study of ischemia-reperfusion in the heart, dynasore protected cardiomyocytes from death due to mitochondrial fragmentation, attributed to inhibition of dynamin family member DRP1 (12). Another study showed a neuroprotective effect of dynasore after spinal cord injury, also attributed to inhibition of DRP1 (13). As a third example, dynasore has been demonstrated to have a variety of growth-inhibitory effects on cancer cells that are independent of classic dynamins, but the molecular targets have not been identified (14, 15).

Damage due to many noxious agents that cause ocular surface damage, such as pathogens, toxins, ultraviolet light and chemicals, is exacerbated by oxidative stress (16–20). Oxidative

stress has been implicated in dry eye and other ocular surface disorders (17, 21, 22). In a recent study, we investigated mechanisms of vital dye uptake stimulated by exposure to an oxidant using a cell culture model of human corneal epithelial cells with mucosal differentiation, and an organ culture model of ex vivo mouse eyes. We made the surprising discovery that dynasore protects cells, as demonstrated by assays of metabolic activity and plasma membrane integrity, while also maintaining the transcellular barrier by protection of the mucosal glycocalyx (23). These results suggest that dynasore targets signaling pathways activated in response to oxidative agent exposure that cause cell and glycocalyx damage.

Oxidative stress leads to endoplasmic reticulum (ER)[1] stress, which activates the unfolded protein response (UPR) (24). The UPR monitors ER conditions, sensing an insufficiency in the protein-folding capacity (and hence the threat of misfolding) and communicates this information to gene expression programs. The UPR is protective if stress is not excessive. However, persistent accumulation of misfolded proteins and prolonged activation of the UPR promotes programmed cell death (25–27).

The UPR is orchestrated by three sensors situated in the ER membrane representing the three UPR branches: Activating Transcription Factor 6 or ATF6, Inositol-requiring enzyme 1 or IRE1 (Hugo nomenclature: ERN1), and PKR like ER kinase or PERK (Hugo nomenclature: EIF2AK3). These sensors are kept inactive by the molecular chaperone GRP78 (Hugo nomenclature: HSPA5). When the ER is stressed, GRP78 releases the sensors in favor of binding to misfolded proteins. Each activated sensor produces a unique transcription factor: ATF6 produces a proteolytically-cleaved form of ATF6 called ATF6(N), IRE1 produces an unconventionally spliced form of the X Box Binding Protein 1 (XBP1) transcription factor called sXBP1, and PERK produces ATF4. Gene expression elicited by these transcription factors leads to increased protein-folding capacity. IRE1 and PERK also decrease the load of proteins entering the ER in a variety of ways, e.g., phosphorylation of translation factor eIF2α (HUGO nomenclature: EIF2S1). Both outcomes work as feedback loops that mitigate ER stress (27). Cell death is mainly coordinated by the PERK branch of the UPR through downstream transcription factor CHOP (HUGO nomenclature: DDIT3). CHOP can down-regulate pro-survival proteins (like Bcl-2) while increasing the expression of pro-death factors (28).

Ca^{2+} acts as a second messenger regulating vital cellular processes. Physiological stimulation of G-protein coupled receptors associated with the inositol-1,4,5-triphosphate (IP3) and phospholipase C cascade activates ER-localized IP3 receptors leading to Ca^{2+} release (29). After the initial receptor-initiated Ca^{2+} transient, a sustained Ca^{2+} influx from the extracellular milieu occurs that provides prolonged Ca^{2+} signals and allows ER store refilling. ER stress disrupts this Ca^{2+} homeostatic mechanism, resulting in the release of Ca^{2+} from the ER to the cytosol and to the mitochondria (30, 31), along with UPR activation (29).

[1]The non-standard abbreviations are: ANOVA: Analysis of Variance: DMEM/F12: Dulbecco's Modified Eagle Medium: Nutrient Mixture F-12; ER: endoplasmic reticulum; HCLE: Human Corneal Limbal Epithelial; IP3: inositol-1,4,5-triphosphate; KSFM: keratinocyte serum free medium; mPTP: mitochondrial permeability transition pore; qRT-PCR: quantitative real-time polymerase chain reaction; tBHP: tert-butyl hydroperoxide; UPR: unfolded protein response

The goal of this study was to uncover the mechanism behind the protective effect of dynasore on mucosal ocular surface epithelia. We applied our cell culture model to determine whether the UPR was activated by exposure to an oxidant, and whether this might be modulated by dynasore. We report the very novel finding that Dynasore protects ocular surface mucosal epithelia subjected to oxidative stress by maintaining Ca^{+2} homeostasis, thereby inhibiting the PERK branch of the UPR that promotes cell death via CHOP.

Results

Dynasore, but not the DRP1 inhibitor mdivi-1, protects mitochondria in HCLE cells subjected to oxidative stress; DRP1 inhibition also fails to protect transcellular barriers.

The protective effect of dynasore on cells subjected to oxidative stress has been traced in some models to its capacity to prevent mitochondrial fragmentation by inhibition of the dynamin family GTPase DRP1 (12, 13). We attempted to determine whether this was also the mechanism for protection of corneal epithelial cells. To create an environment of oxidative stress, we exposed relatively undifferentiated monolayer cultures of the immortalized human corneal epithelial cell line, HCLE, to the oxidant tert-butyl hydroperoxide (tBHP) for a period of two hours. Some cultures were then left untreated, while others were treated with either dynasore or a selective inhibitor of DRP1, mdivi-1 (32). At the end of the experiment, mitochondrial damage was quantified using the calcein-AM/$CoCl_2$ assay.

Representative results of the experiment are shown in Fig 1A. In the calcein-AM/$CoCl_2$ assay, healthy cells exhibit brightly fluorescent mitochondria, while cells in which mitochondria are damaged leading to opening of the mitochondrial permeability transition pore (mPTP) exhibit a loss of fluorescence. Control cells showed normal mitochondrial staining with calcein, while exposure to tBHP caused loss of calcein fluorescence. Mdivi-1 failed to counter the effects of tBHP at any concentration, while dynasore maintained mitochondrial staining similar to control cells.

Not having observed an effect of mdivi-1 on mitochondria in monolayer cultures subjected to oxidative stress, we moved on to focus on mdivi-1 effects using stratified cultures of Human Corneal Limbal Epithelial (HCLE) cells with mucosal differentiation. These cultures model additional features of the ocular surface in vivo. Cells of the apical stratified layer exhibit squamous morphology/physiology; these flattened cells are connected by tight junctions to form the paracellular barrier and they also elaborate a mucosal transcellular barrier. Significantly, they are in the final stages of life and may be differentially vulnerable to damaging stress. In addition to the calcein-AM/$CoCl_2$ assay to quantify mitochondrial damage, we also used two assays for transcellular barrier function for this experiment: 1) the trypan blue exclusion assay to quantify integrity of the plasma membrane barrier and 2) the rose bengal exclusion assay to quantify integrity of the mucosal barrier. In these assays, dye exclusion is evidence of barrier integrity.

Representative results of this experiment are shown in Fig 1B–D. As in the monolayer cultures, treatment with mdivi-1 at 50 μM and 100 μM could not rescue cells from the effects of tBHP exposure. All cells exposed to tBHP exhibited lower calcein fluorescence,

indicating mPTP opening (Fig 1B). All cells exposed to tBHP also exhibited higher trypan blue (Fig 1C) and rose bengal (Fig 1D) staining, indicating damage to the transcellular barriers.

We conclude that dynasore protects mitochondrial function in corneal epithelial cells subjected to oxidative stress; this is independent of DRP1. Inhibition of DRP1 also failed to protect transcellular barriers.

Dynasore and the RIPK1 inhibitor necrostatin-1 protect mitochondria and the plasma membrane barrier in HCLE cells subjected to oxidative stress, but only dynasore protects the mucosal barrier

In order to unravel the mechanism-of-action for dynasore, we found it necessary to better understand the mechanisms of corneal epithelial cell damage in our oxidative stress model. In our previous work (23), we showed that cells exposed to tBHP for two hours expressed ANXA5, an early marker for various forms of programmed cell death (33). Exposure of cultured endothelial cells to tBHP has been reported by others to induce programmed cell death by either apoptosis or necroptosis, depending on the concentration of tBHP used (34). Following up on this observation, we treated monolayer cultures of HCLE cells subjected to oxidative stress with Z-VAD-FMK (a pan-caspase inhibitor), targeting apoptosis, or necrostatin-1 (a RIPK1 inhibitor), targeting lytic pathways of cell death such as necroptosis or pyroptosis.

Representative results of this experiment are shown in Fig 2. Once again applying the calcein-AM/$CoCl_2$ assay, we found significantly lower mitochondrial fluorescence with all concentrations of Z-VAD-FMK in cells subjected to oxidative stress, as compared to control cells, and similar to cells subjected to oxidative stress, but otherwise untreated (Fig 2A and C). Low concentrations of necrostatin-1 did not prevent the loss of fluorescence. However, at 300 μM, necrostatin-1 completely prevented the loss of fluorescence (Fig 2A and B).

Having identified the capacity of necrostatin-1 to protect mitochondria in monolayer cultures subjected to oxidative stress, we compared its activity to dynasore in stratified HCLE cells with mucosal differentiation. Representative results of this experiment are shown in Fig 3. Both necrostatin-1 and dynasore blocked the loss of calcein fluorescence. Interestingly however, necrostatin-1 had only selective effects on transcellular barrier function. Like dynasore, necrostatin-1 maintained trypan blue exclusion, indicating maintenance of plasma membrane integrity (Fig 3A and B). However, only dynasore maintained rose bengal exclusion indicative of mucosal barrier integrity (Fig 3C).

We conclude that corneal epithelial cells subjected to oxidative stress enter a lytic pathway for programmed cell death controlled by RIPK1, and this is blocked by both the specific RIPK1 inhibitor, necrostatin-1, as well as dynasore. Both necrostatin-1 and dynasore also maintain the plasma membrane transcellular barrier. However, only dynasore maintains the mucosal transcellular barrier.

The UPR is activated in HCLE cells subjected to oxidative stress; dynasore inhibits the UPR PERK branch

Oxidative stress can lead to ER stress, which activates the UPR (24). We hypothesized that the UPR is activated in corneal epithelial cells subjected to oxidative stress and that dynasore could inhibit this process.

To detect UPR activation in stratified HCLE cells with mucosal differentiation, we exposed these cultures to tBHP, then performed assays to detect UPR branch markers. Representative results are shown in Fig 4. An increase in the mRNA for the spliced form of *XBP1* (*sXBP1*) is specific for IRE1 branch activation (Fig 4A), and a reliable indirect method of determining IRE1 activation (35, 36). We observed a significant increase in *sXBP1* mRNA in tBHP-stressed cells as compared to controls, as determined by quantitative real-time Polymerase Chain Reaction (qRT-PCR) (Fig 4B). Dynasore had no effect on activation of this pathway in tBHP-stressed cells.

As a marker for the PERK branch, we used *CHOP* mRNA (Fig 4A). *CHOP* mRNA was also elevated in the tBHP-stressed group (Fig 4B). However, in contrast to *sXBP1* mRNA, *CHOP* mRNA was decreased in the tBHP-stressed group when dynasore was added.

Western blot analysis demonstrated increased phosphorylation of eIF2α in the tBHP-stressed group, another marker of the PERK branch, while tBHP-stressed cells treated with dynasore had similar levels of P-eIF2α than control cells (Fig 4C).

We conclude that the UPR is activated in corneal epithelial cells subjected to oxidative stress, and that dynasore selectively inhibits the PERK branch of the response.

Dynasore inhibits the intracellular [Ca^{2+}] increase responsible, at least in part, for UPR PERK branch activation in HCLE cells subjected to oxidative stress

An increase in cytosolic Ca^{2+} also activates the UPR, inducing autophosphorylation of PERK (37, 38). An increase in cytosolic Ca^{2+} can occur either as a direct consequence of oxidative stress or after UPR activation (39, 40). We hypothesized that dynasore could be acting on Ca^{2+} homeostasis to inhibit the PERK pathway.

First, we investigated effects of dynasore on Ca^{2+} dynamics in HCLE cells subjected to oxidative stress. We used monolayer cultures of HCLE cells for these experiments, as calcium fluctuations may differ in cells of different layers, masking single cell responses. We monitored Ca^{2+} concentration ([Ca^{2+}]) after exposure to tBHP, using the probe Fluoro-4 and live cell imaging. Representative results are shown in Fig 5. Exposure of cells to tBHP induced a dramatic increase in [Ca^{2+}], which was not observed in control cells (Fig 5A and Movies S1 and S2). When treated with dynasore, tBHP-stressed cells did not exhibit the [Ca^{2+}] increase (Movie S3). Significantly, treatment with necrostatin-1 at a concentration that we have already shown protects mitochondria (see Fig 2A), failed to prevent the [Ca^{2+}] increase in tBHP-stressed cells (Movie S4).

To determine whether elevated [Ca^{2+}] was a cause of PERK pathway activation, cultures of stratified HCLE cells with mucosal differentiation were exposed to tBHP while also being

treated with BAPTA-AM, a cell-permeable Ca^{2+} chelator. The use of BAPTA-AM inhibited the increase in CHOP expression caused by cell culture exposure to tBHP (Fig 5B), as well as the increase in eIF2α phosphorylation (Fig 5C).

We conclude that dynasore inhibits the intracellular [Ca^{2+}] increase responsible, at least in part, for UPR PERK branch activation in corneal epithelial cells subjected to oxidative stress.

Discussion

The ocular surface is a unique mucosal compartment in which anatomical, physiological and immunological features act to foster a protective microenvironment (41). Nevertheless, epithelial cells and their mucosal glycocalyx remain vulnerable to the external environment (1). Response to damaging stimuli is exacerbated by induction of oxidative stress, which has been implicated in ocular surface disorders (16–22). Recently, we made the surprising discovery that dynasore prevents damage to the cells and their mucosal glycocalyx subjected to oxidative stress in a cell culture model of stratified human corneal epithelial cells with mucosal differentiation, and in an organ culture model of ex vivo mouse eyes (23). Here we report that exposure to the oxidant tBHP activates the UPR in our cell culture model, and that dynasore acts selectively to inhibit the PERK branch, which coordinates cell death. Furthermore, we provide evidence for a regulatory role of dynasore in Ca^{2+} dynamics as the mechanism to achieve this effect, thus shifting the UPR towards homeostasis. To our knowledge, this is the first time that dynasore has been shown to have an effect on the UPR.

Developed by Macia et al (2006) to inhibit the GTPase activity of classic dynamins, dynasore has provided a valuable tool in the study of endocytosis. In the original report (6), dynasore was found to inhibit the GTPase activity of DNM1 and DNM2 with an IC_{50} of 15uM, but also inhibited activity of DRP1, another dynamin family member, with an IC_{50} of 80uM. Targeting of DRP1, a member of the mitochondrial-localized dynamin-like subfamily, appears to be responsible for the cytoprotective effects of dynasore in several different models (12, 13, 42, 43). In the current study, we explored the effects of inhibiting DRP1 using the small molecule mdivi-1, which inhibits DRP1 selectively, and also blocks mitochondrial division (32). Mdivi-1 is cytoprotective and exhibits therapeutic potential in preclinical models (12, 42, 44). However, our results showed that mdivi-1 did not protect HCLE cells from oxidative stress damage, leading us to conclude that dynasore must be acting on some other target.

Previously, we showed that corneal epithelial cells exposed to tBHP were positive for ANXA5 (23), an early marker for programmed cell death. Thus, a reasonable point for starting the search for a dynasore target were the various programmed cell death pathways. Here, in a comparison of the pan-caspase inhibitor Z-VAD-FMK or the RIPK1 inhibitor necrostatin-1, we show that only necrostatin-1 protects mitochondria. Caspases are apoptotic effectors that usually ensure immunological silence. In contrast, RIPK1 is an effector of lytic pathways such as necroptosis and pyroptosis (45, 46), that can induce potent inflammatory responses in vivo (47). Studies have shown both the activation of necroptosis (48–50) and the inflammasome (51–53) in ocular surface disease. Significantly, inhibition of RIPK1

failed to preserve mucosal barrier function in our cell culture model, unlike dynasore. Given these results, dynasore is either acting on two different processes, or at an upstream event that can lead to both necroptosis and mucosal barrier dysfunction.

Typically elicited by accumulation of unfolded proteins in the ER, the UPR has received much recent attention for its role in numerous disease processes (54). Mucosal epithelia seem to be especially sensitive, when the exigencies for producing high amounts of mucins overwhelm the capacity of the ER (24, 55–58). Oxidative stress products like 4-hydroxynonenal (4-HNE), can induce modifications in molecular chaperones, making them inactive, thus also causing ER stress (59).

In the present study, we show that exposure to tBHP activates the UPR in stratified cultures of HCLE cells with mucosal differentiation, as demonstrated by the increase in markers for the IRE1 and PERK pathways: *sXBP1* and *CHOP* mRNA, as well as eIF2α phosphorylation. Significantly, treatment with dynasore did not affect activation of the IRE1 branch of the UPR, but did inhibit activation of the PERK branch, which coordinates cell death (25–27, 40, 60, 61).

Besides direct ER stress, the PERK pathway can be activated by disturbances in Ca^{2+} dynamics; either a decrease in ER Ca^{2+} or an increase in cytosolic Ca^{2+} are related to increased phosphorylation of PERK (37, 38). Our results demonstrate that exposure to tBHP causes a persistent increase in intracellular Ca^{2+}. This increase was absent when cells were treated with dynasore. Moreover, the use of the Ca^{2+} chelator BAPTA-AM prevented the increase in *CHOP* mRNA and eIF2α phosphorylation, showing that targeting the increase in Ca^{2+} can reduce activity of this UPR branch.

Accumulating evidence suggests that the UPR plays a role in ocular surface disease, providing support for the in vivo validity of our results. UPR activation in salivary glands plays an essential role in dry mouth associated with Sjögren syndrome, an autoimmune disease that also affects the lacrimal gland (62). In the Sjögren syndrome lacrimal gland, activation of HIF1A, which is known to stimulate UPR activity, prevents acinar cell death (63). The UPR is also activated in conjunctival goblet cells by IFNG in Sjögren syndrome, and this has been causally linked to mucin deficiency and tear dysfunction (64). Systemic ER stress in mice results in reduced tear secretion and damage to the ocular surface epithelia (65). Very recently, one of our labs reported positive reactivity of GRP78 in conjunctival epithelium of patients with ocular cicatricial pemphigoid, and increased levels of GRP78 and sXBP1 in human corneal epithelial cells treated with TNFα (66).

Calcium and mitochondrial homeostasis integrate into multiple mechanistic pathways for disease. Ca^{2+} dynamics in corneal epithelium have been investigated in corneal wound healing studies (67–70). An increase in cytosolic Ca^{2+} can be a direct effect of oxidative stress, as it can provoke the aberrant activation of store operated Ca^{2+} channels (SOC) when the accumulation of the oxidized form of glutathione causes S-glutathionylation of Stromal Interaction Molecule 1 (STIM1) (39). On the other hand, ER stress can induce the release of Ca^{2+} from the ER to the cytosol, as well as a Ca^{2+} flux from the ER to the mitochondria (30, 31), which, if sustained, can have disastrous consequences for the latter.

Having identified key pathways whereby dynasore protects the ocular surface epithelia subjected to oxidative stress, the next step in our work will be to determine the direct molecular target(s) of dynasore inhibition of which lead to protection of mucosal ocular surface epithelial cells and their glycocalyx. We believe it is likely that targets will be found among the dynamin family. Classic dynamins have been connected with opening of L-type Ca^{2+} channels gonadotropin-releasing hormone (GNRH1) via association with cortactin and the actin cytoskeleton (71). Dynasore has previously been shown to block Ca^{2+} release from internal sources induced by VEGFR2. This effect was independent of the classic dynamins, but might involve other dynamin family members (8). The atlastins, distant members of the dynamin family, were found to have a role in the activation of SOC (72). Importantly, dynasore inhibits atlastin-1 (ATL1)-induced vesicle formation in vitro, although this requires a much higher dynasore concentration than needed to inhibit the GTPase activity of classic dynamins (73). Mitofusin-2 (MFN2), another dynamin-like GTPase, is required for mitochondrial Ca^{2+} uptake through its role in ER-mitochondria tethering (29, 74–76). Mobilization of Ca^{2+} from the ER to the mitochondria via IP3Rs is common in ER stress, when GPR78 dissociates from Sig-1Rs and can result in cytosolic Ca^{2+} increase (77).

In summary, we have uncovered some key processes involved in cellular damage due to oxidant exposure, the inhibition of which leads to a better outcome for the mucosal epithelium of the ocular surface. Given the present results, new strategies can be developed to alleviate ER stress and protect the ocular surface. Addressing Ca^{2+} might be a good strategy to maintain the homeostatic face of the UPR while preventing cell death. Our findings that dynasore has the potential to prevent cell death and alleviate ER stress by restoring Ca^{2+} homeostasis tightens the net around specific targets that are central to these processes. These results might lead to a new scenario where dynasore or related chemical analogs emerge as new therapeutic agents.

Material and Methods

Cell culture model

A telomerase-immortalized human corneal limbal epithelial (HCLE) cell line was used as previously described (78). The cell line was derived from normal tissue and expresses the same mucin gene and keratin repertoire as native epithelia when stimulated to differentiate (78). The cell line was authenticated by marker expression analysis (79) and characterization of polymorphic short tandem repeat (STR) loci (78, 80).

Monolayer cultures were used for first approaches to determine any cytoprotective effect of the treatment agents. Here, cells were grown in keratinocyte serum free medium (KSFM; Thermo Fisher Scientific, Waltham, MA) containing 25 μg/mL bovine pituitary extract, 0.2 ng/mL epithelial growth factor (EGF) and 0.4 mM $CaCl_2$. Experiments were performed with sub-confluent cultures.

Stratified HCLE cells with mucosal differentiation were used to model additional features of the ocular surface in vivo, as cells of the apical stratified layer exhibit squamous morphology/physiology and also elaborate a mucosal transcellular barrier. HCLE cells were induced to stratify and differentiate as previously described (78). Briefly, HCLE cells were

grown in KSFM (supplemented as described above) until the monolayer was confluent. Then, cells were switched to Dulbecco's Modified Eagle Medium: Nutrient Mixture F-12 (DMEM/F12) medium supplemented with 15 mM HEPES, 2 mM L-glutamine, 10% calf serum and 10 ng/mL EGF (Thermo Fisher Scientific) for 7 days before performing the experiments. Stratification was routinely evaluated using phase contrast microscopy; differentiation leading to mucosal transcellular barrier function was evaluated using the rose bengal penetration assay. Use of these assays has been previously described by one of our labs (81).

Oxidative stress and cell treatment

To create an environment of oxidative stress, cells were exposed to tert-butyl hydroperoxide (tBHP), as we have previously described (23). To investigate mechanisms of cell damage, groups of tBHP-stressed cultures were left untreated, or treated with dynasore or chemical inhibitors of different processes: mdivi-1 (mitochondrial division), necrostatin-1 (necroptosis), Z-VAD-FMK (pan-caspases inhibitor) or BAPTA-AM (Ca^{2+} chelator) (all from Sigma-Aldrich, St. Louis, MO). Inhibitors were diluted into culture medium from concentrated stock solutions dissolved in DMSO.

For experiments with monolayer HCLE cell cultures, cells were grown to 90% confluence. Then, cells were pre-incubated for 1 hour in DMEM/F12 with different concentrations of the specified inhibitor (as indicated in text below), 40 μM dynasore hydrate (Sigma-Aldrich, St. Louis, MO), or the same amount of their solvent, DMSO. Then, cells were switched to the same medium with 1 mM tBHP and incubated for 2 hours. At the end of the experiment, one or more bioassays were performed as described below.

For experiments with stratified HCLE cell cultures with mucosal differentiation, cells were cultured as described and treated at the 7^{th} day of stratification. Cells were serum-starved for 1 hour in DMEM/F12. Then cells were pre-incubated for 1 hour with the inhibitors and tBHP-stressed for 2 hours as described for monolayer cultures. Concentrations of 80 μM dynasore and 10 mM tBHP were used in this case. After this, one or more bioassays were performed as described below.

Mitochondrial permeability transition pore (mPTP) assay

The calcein-AM/$CoCl_2$ assay was used to evaluate mPTP opening, performed with the Image-iT ™ LIVE Mitochondrial Permeability Transition Pore Assay Kit (Cat. No. I35103; Thermo Fisher Scientific). In this assay, cells are loaded with calcein-AM, which accumulates in cytosolic compartments. Endogenous esterases liberate the very polar fluorescent dye calcein, however, $CoCl_2$ quenches its fluorescence throughout the cell. The exception is the mitochondria, where the electrochemical gradient prevents $CoCl_2$ entry. However, opening of the mPTP alters mitochondrial permeability and permits fluorescence quenching (82).

Cells were washed twice with modified HBSS (Hank's Balanced Salt Solution supplemented with 10 mM HEPES, 2 mM L-glutamine and 100 μM succinate) and incubated with 1 μM calcein-AM and 1 mM $CoCl_2$ at 37 °C for 30 min (for monolayer cultures) or 45 min (for stratified cultures with mucosal differentiation). After 3 washes with

modified HBSS, images were obtained with a microscope equipped with epifluorescence (Lionheart FX automated microscope, BioTek Instruments, Winooski, VT) and then analyzed to get a measurement of fluorescence intensity (Gen5 3.0, BioTek).

Trypan blue exclusion assay

The trypan blue exclusion assay measures plasma membrane transcellular barrier integrity, as trypan blue can enter cells only through breeches in the plasma membrane (83). The assay was performed as described (83). Cells were washed twice in PBS (without Ca^{2+}). Then, cells were incubated in 0.4% Trypan Blue (Thermo Fisher Scientific) for 4 minutes at room temperature and washed 3 times in PBS. After imaging, the cells were incubated in DMSO for 1 hour at room temperature and the absorbance was read at 590 nm using Synergy H1 microplate reader (BioTek Instruments).

Rose bengal exclusion assay

The rose bengal exclusion assay measures mucosal transcellular barrier integrity. Corneal epithelial cells in culture exclude rose bengal if induced to differentiate and elaborate a mucosal glycocalyx, and rose bengal staining is indicative of breeches in the mucosal barrier (1). To perform the assay, cells were washed twice in PBS (without Ca^{2+}), incubated in 0.1% rose bengal (Sigma-Aldrich) for 5 minutes at room temperature, then washed 3 times in PBS. Cells were then photographed. After imaging, the cells were incubated in DMSO for 1 hour at room temperature and the absorbance was read at 562 nm using a Synergy H1 microplate reader (BioTek).

RNA isolation and quantitative real-time Polymerase Chain Reaction (qRT-PCR)

mRNA for two UPR branch markers employed in this study, *sXBP1* and *CHOP*, were detected and quantified by qRT-PCR. For *sXBP1* mRNA, primers were designed to span the 26-base pair intron that is removed by IRE1, thus making them specific for the spliced mRNA species derived from the *XBP1* gene, as previously described by one of our labs (66). Primers are listed in Table 1.

RNA was isolated from stratified HCLE cells using GeneJET RNA Purification Kit (Thermo Fisher Scientific) following the manufacturer's instructions and using PureLink® DNase Set (Invitrogen, Carlsbad, CA) to remove DNA contamination from columns. First-strand cDNA was synthesized from 1 μg of total RNA using a reverse transcription kit (High Capacity Reverse Transcription Kit; Applied Biosystems, Foster City, CA), in accordance with the manufacturer's instructions.

The qRT-PCR reaction was performed using SYBR® Green reagents (iTaq Universal SYBR Green Supermix, Bio-Rad, Hercules, CA) with specific primers (Table 1). The following parameters were used: 30 s at 95 °C, followed by 40 cycles of 5 s at 95 °C and 30 s at 60 °C. All samples were normalized to RNA levels of the housekeeping gene *ACTB* (Table 1). The comparative CT method was used for relative quantitation, selecting the relative amount in control cells as the calibrator.

Protein isolation and western blot

Western blotting was used to determine relative phosphorylation of eIF2α, which serves as a marker for activation of the UPR PERK branch of the UPR. The protein eIF2α is one subunit of the multimer eIF2, which is a heterotrimer of 126 kDa. The complex dissociates when dissolved in SDS sample buffer. The molecular weight of eIF2α is 36 kDa.

Stratified HCLE cells were lysed in RIPA buffer (VWR Scientific) containing protease and phosphatase inhibitor cocktail (Thermo Fisher Scientific) and harvested using a cell scraper. The lysates were centrifuged at 14000 *X g* for 15 min at 4°C. Supernatant were collected and protein concentration was assessed (Synergy H1 microplate reader, BioTek).

Protein extracts (60 μg per sample) were loaded on SDS-PAGE gels (Bio-Rad) under reducing conditions. Membranes were blocked in TBS buffer containing 0.1% Tween and 5% BSA for 1 h at room temperature and then incubated with anti-eIF2α, anti-P-eIF2α (both at 1:1000; Cat. No. 5324S and Cat. No. 3398S, respectively; Cell Signaling Technologies, Danvers, MA) or anti-β-actin (ACTB) (1:4000; Cat. No. 12262; Cell Signaling) overnight at 4°C.

Incubation with secondary antibodies bound to IR dyes (Li-Cor Biosciences, Lincoln, NE) were performed for 1 h at room temperature. The membranes were visualized using a Li-Cor Odyssey Imaging System (Li-Cor Biosciences). The density of different bands was assessed using Image J software (National Institutes of Health, Bethesda, MD).

Calcium assay

Subconfluent monolayer cultures of HCLE cells were loaded with Fluo-4 Direct™, with a final probenecid concentration of 2.5 mM (Cat. No. F10471; Thermo Fischer Scientific), for 60 min at 37°C. Then, tBHP with either DMSO, dynasore (40 μM) or necrostatin-1 (300 μM) were added. Time-lapse images were obtained with a fluorescent microscope (Lionheart FX automated microscope, BioTek) attached to a source of CO_2 (controlled to keep 5% of CO_2) and the temperature was kept at 37°C. Images were then analyzed to get a measurement of fluorescence intensity (Gen5 3.0, BioTek). Images were taken every 10 min during the 2 h of exposure to tBHP.

Statistical analysis

Statistical analysis was performed using GraphPad Prism 5 (GraphPad Software). The Kolmogorov-Smirnov test was used to assess the normality of data distribution and Bartlett's test for the homogeneity of the variances. Based on normality of the data distribution and the homogeneity of the variances, Analysis of Variance (ANOVA) with Bonferroni's post-hoc test or the Kruskal-Wallis test with Dunn's post-hoc test was applied for comparison, as indicated in the figure legends. P value < 0.05 was considered statistically significant.

Supplementary Material

Refer to Web version on PubMed Central for supplementary material.

Acknowledgments:

The authors thank I. K. Gipson for providing the human corneal epithelial cell line. They are also grateful to A. M. Woodward for assistance in the technical development of the project.

Funding: This work was supported by NIH grant R01EY026479 (to M.E.F.). Further support was provided by grants from Research to Prevent Blindness, Inc. and from the Massachusetts Lions Eye Research Fund (to the Department of Ophthalmology, Tufts University School of Medicine).

References

1. Gipson IK, The Ocular Surface: The Challenge to Enable and Protect Vision. Invest. Ophthalmol. Vis. Sci 48, 4383–4389 (2007). [PubMed: 17898254]
2. Sugrue SP, Zieske JD, ZO1 in corneal epithelium: association to the zonula occludens and adherens junctions. Exp. Eye Res 64, 11–20 (1997). [PubMed: 9093016]
3. Fini ME, Jeong S, Gong H, Martinez-Carrasco R, Laver NMV, Hijikata M, Keicho N, Argüeso P, Membrane-associated mucins of the ocular surface: New genes, new protein functions and new biological roles in human and mouse. Prog. Retin. Eye Res 75, 100777(2020). [PubMed: 31493487]
4. Mantelli F, Argüeso P, Functions of ocular surface mucins in health and disease. Curr. Opin. Allergy Clin. Immunol 8, 477–483 (2008). [PubMed: 18769205]
5. Woodward AM, Mauris J, Argüeso P, Binding of transmembrane mucins to galectin-3 limits herpesvirus 1 infection of human corneal keratinocytes. J. Virol 87, 5841–7 (2013). [PubMed: 23487460]
6. Macia E, Ehrlich M, Massol R, Boucrot E, Brunner C, Kirchhausen T, Dynasore, a Cell-Permeable Inhibitor of Dynamin. Dev. Cell 10, 839–850 (2006). [PubMed: 16740485]
7. Park RJ, Shen H, Liu L, Liu X, Ferguson SM, De Camilli P, Dynamin triple knockout cells reveal off target effects of commonly used dynamin inhibitors. J. Cell Sci 126, 5305–5312 (2013). [PubMed: 24046449]
8. Basagiannis D, Zografou S, Galanopoulou K, Christoforidis S, Dynasore impairs VEGFR2 signalling in an endocytosis-independent manner. Sci. Rep 7, 1–11 (2017). [PubMed: 28127051]
9. Persaud A, Cormerais Y, Pouyssegur J, Rotin D, Dynamin inhibitors block activation of mTORC1 by amino acids independently of dynamin. J. Cell Sci 131, 1–11 (2018).
10. Preta G, Cronin JG, Sheldon IM, Dynasore - Not just a dynamin inhibitor. Cell Commun. Signal 13, 1–7 (2015). [PubMed: 25589173]
11. Praefcke GJK, McMahon HT, The dynamin superfamily: universal membrane tubulation and fission molecules? Nat. Rev. Mol. Cell Biol 5, 133–147 (2004). [PubMed: 15040446]
12. Gao D, Zhang L, Dhillon R, Hong TT, Shaw RM, Zhu J, Dynasore Protects Mitochondria and Improves Cardiac Lusitropy in Langendorff Perfused Mouse Heart. PLoS One. 8, 1–10 (2013).
13. Li G, Shen F, Fan Z, Wang Y, Kong X, Yu D, Zhi X, Lv G, Cao Y, Dynasore Improves Motor Function Recovery via Inhibition of Neuronal Apoptosis and Astrocytic Proliferation after Spinal Cord Injury in Rats. Mol. Neurobiol 54, 7471–7482 (2017). [PubMed: 27822712]
14. Wang T, Wang D, Zhang Y, Zhang J, Sun X, Wu Y, Wang S, Zhang Y, Xu L, Kong Q, Gao Y, Wu Y, Liu F, Liu S, Zhang Y, Lei T, Liu H, Dynasore-induced potent ubiquitylation of the exon 19 deletion mutant of epidermal growth factor receptor suppresses cell growth and migration in non-small cell lung cancer. Int. J. Biochem. Cell Biol 105, 1–12 (2018). [PubMed: 30268747]
15. Zhong B, Shi D, Wu F, Wang S, Hu H, Cheng C, Qing X, Huang X, Luo X, Zhang Z, Shao Z, Dynasore suppresses cell proliferation, migration, and invasion and enhances the antitumor capacity of cisplatin via STAT3 pathway in osteosarcoma. Cell Death Dis. 10 (2019), doi:10.1038/s41419-019-1917-2.
16. Dogru M, Kojima T, Simsek C, Tsubotav K, Potential role of oxidative stress in ocular surface inflammation and dry eye disease. Investig. Ophthalmol. Vis. Sci 59, DES163–DES168 (2018). [PubMed: 30481822]
17. Cejka C, Cejkova J, Oxidative stress to the cornea, changes in corneal optical properties, and advances in treatment of corneal oxidative injuries. Oxid. Med. Cell. Longev 2015 (2015), doi:10.1155/2015/591530.

18. Deng R, Hua X, Li J, Chi W, Zhang Z, Lu F, Zhang L, Pflugfelder SC, Li DQ, Oxidative stress markers induced by hyperosmolarity in primary human corneal epithelial cells. PLoS One. 10, 1–16 (2015).
19. Dai Y, Zhang J, Xiang J, Li Y, Wu D, Xu J, Calcitriol inhibits ROS-NLRP3-IL-1β signaling axis via activation of Nrf2-antioxidant signaling in hyperosmotic stress stimulated human corneal epithelial cells. Redox Biol. 21, 101093(2019). [PubMed: 30611121]
20. Chi W, Hua X, Chen X, Bian F, Yuan X, Zhang L, Wang X, Chen D, Deng R, Li Z, Liu Y, de Paiva CS, Pflugfelder SC, Li DQ, Mitochondrial DNA oxidation induces imbalanced activity of NLRP3/NLRP6 inflammasomes by activation of caspase-8 and BRCC36 in dry eye. J. Autoimmun 80, 65–76 (2017). [PubMed: 28238526]
21. Seen S, Tong L, Dry eye disease and oxidative stress. Acta Ophthalmol. 96, e412–e420 (2018). [PubMed: 28834388]
22. Shoham A, Hadziahmetovic M, Dunaief JL, Mydlarski MB, Schipper HM, Oxidative stress in diseases of the human cornea. Free Radic. Biol. Med 45, 1047–1055 (2008). [PubMed: 18718524]
23. Webster A, Chintala SK, Kim J, Ngan M, Itakura T, Panjwani N, Argüeso P, Barr JT, Jeong S, Fini ME, Dynasore protects the ocular surface against damaging oxidative stress. PLoS One. 13, e0204288(2018). [PubMed: 30303976]
24. Chong WC, Shastri MD, Eri R, Endoplasmic reticulum stress and oxidative stress: A vicious nexus implicated in bowel disease pathophysiology. Int. J. Mol. Sci 18, 1–19 (2017).
25. Grootjans J, Kaser A, Kaufman RJ, Blumberg RS, The unfolded protein response in immunity and inflammation. Nat. Rev. Immunol 16, 469–484 (2016). [PubMed: 27346803]
26. Zhu P, Hu S, Jin Q, Li D, Tian F, Toan S, Li Y, Zhou H, Chen Y, Ripk3 promotes ER stress-induced necroptosis in cardiac IR injury: A mechanism involving calcium overload/XO/ROS/mPTP pathway. Redox Biol. 16, 157–168 (2018). [PubMed: 29502045]
27. Walter P, Ron D, The Unfolded Protein Response: From Stress Pathway to Homeostatic Regulation. Science (80-.). 334, 1081–1086 (2011).
28. Rozpedek W, Pytel D, Mucha B, Leszczynska H, Diehl JA, Majsterek I, The Role of the PERK/eIF2α/ATF4/CHOP Signaling Pathway in Tumor Progression During Endoplasmic Reticulum Stress. Curr. Mol. Med 16, 533–544 (2016). [PubMed: 27211800]
29. Krebs J, Agellon LB, Michalak M, Ca2+ homeostasis and endoplasmic reticulum (ER) stress: An integrated view of calcium signaling. Biochem. Biophys. Res. Commun 460, 114–121 (2015). [PubMed: 25998740]
30. Bravo R, Gutierrez T, Paredes F, Gatica D, Rodriguez AE, Pedrozo Z, Chiong M, Parra V, Quest AFG, Rothermel BA, Lavandero S, Endoplasmic reticulum: ER stress regulates mitochondrial bioenergetics. Int. J. Biochem. Cell Biol 44, 16–20 (2012). [PubMed: 22064245]
31. Xiao WC, Zhang J, Chen SL, Shi YJ, Xiao F, An W, Alleviation of palmitic acid-induced endoplasmic reticulum stress by augmenter of liver regeneration through IP3R-controlled Ca2+ release. J. Cell. Physiol 233, 6148–6157 (2018). [PubMed: 29323715]
32. Manczak M, Kandimalla R, Yin X, Reddy PH, Mitochondrial division inhibitor 1 reduces dynamin-related protein 1 and mitochondrial fission activity. Hum. Mol. Genet 28, 177–199 (2019). [PubMed: 30239719]
33. Kroemer G, Galluzzi L, Vandenabeele P, Abrams J, Alnemri ES, Baehrecke EH, Blagosklonny MV, El-Deiry WS, Golstein P, Green DR, Hengartner M, Knight RA, Kumar S, Lipton SA, Malorni W, Nuñez G, Peter ME, Tschopp J, Yuan J, Piacentini M, Zhivotovsky B, Melino G, Classification of cell death: Recommendations of the Nomenclature Committee on Cell Death 2009. Cell Death Differ. 16, 3–11 (2009). [PubMed: 18846107]
34. Zhao W, Feng H, Sun W, Liu K, Lu JJ, Chen X, Tert-butyl hydroperoxide (t-BHP) induced apoptosis and necroptosis in endothelial cells: Roles of NOX4 and mitochondrion. Redox Biol. 11, 524–534 (2017). [PubMed: 28088644]
35. Van Schadewijk A, Van'T Wout EFA, Stolk J, Hiemstra PS, A quantitative method for detection of spliced X-box binding protein-1 (XBP1) mRNA as a measure of endoplasmic reticulum (ER) stress. Cell Stress Chaperones (2012), doi:10.1007/s12192-011-0306-2.
36. Oslowski CM, Urano F, in Methods in Enzymology (2011).

37. Vervliet T, Kiviluoto S, Bultynck G, in Endoplasmic Reticulum Stress in Health and Disease, Agostinis P, Afshin S, Eds. (Springer Netherlands, Dordrecht, 2012; 10.1007/978-94-007-4351-9_5), pp. 107–142.
38. Bollo M, Paredes RM, Holstein D, Zheleznova N, Camacho P, Lechleiter JD, Calcineurin interacts with PERK and dephosphorylates calnexin to relieve ER stress in mammals and frogs. PLoS One. 5 (2010), doi:10.1371/journal.pone.0011925.
39. Hawkins BJ, Irrinki KM, Mallilankaraman K, Lien YC, Wang Y, Bhanumathy CD, Subbiah R, Ritchie MF, Soboloff J, Baba Y, Kurosaki T, Joseph SK, Gill DL, Madesh M, S-glutathionylation activates STIM1 and alters mitochondrial homeostasis. J. Cell Biol 190, 391–405 (2010). [PubMed: 20679432]
40. Sano R, Reed JC, ER stress-induced cell death mechanisms. Biochim. Biophys. Acta -Mol. Cell Res 1833, 3460–3470 (2013).
41. Barabino S, Chen Y, Chauhan S, Dana R, Ocular surface immunity: Homeostatic mechanisms and their disruption in dry eye disease. Prog. Retin. Eye Res 31, 271–285 (2012). [PubMed: 22426080]
42. Gao D, Yang J, Wu Y, Wang QQ, Wang QQ, Lai EY, Zhu J, Targeting Dynamin 2 as a Novel Pathway to Inhibit Cardiomyocyte Apoptosis Following Oxidative Stress. Cell. Physiol. Biochem (2016), doi:10.1159/000447908.
43. Reddy PH, Reddy TP, Manczak M, Calkins MJ, Shirendeb U, Mao P, Dynamin-related protein 1 and mitochondrial fragmentation in neurodegenerative diseases. Brain Res. Rev 67, 103–118 (2011). [PubMed: 21145355]
44. feng Fan L, you He P, cong Peng Y, hua Du Q, jun Ma Y, xiang Jin J, zhe Xu H, ru Li J, jiang Wang Z, long Cao S, Li T, Yan F, Gu C, Wang L, Chen G, Mdivi-1 ameliorates early brain injury after subarachnoid hemorrhage via the suppression of inflammation-related blood–brain barrier disruption and endoplasmic reticulum stress-based apoptosis. Free Radic. Biol. Med 112, 336–349 (2017). [PubMed: 28790012]
45. Man SM, Karki R, Kanneganti T-D, Molecular mechanisms and functions of pyroptosis, inflammatory caspases and inflammasomes in infectious diseases. Immunol. Rev 277, 61–75 (2017). [PubMed: 28462526]
46. Lawlor KE, Khan N, Mildenhall A, Gerlic M, Croker BA, D'Cruz AA, Hall C, Kaur Spall S, Anderton H, Masters SL, Rashidi M, Wicks IP, Alexander WS, Mitsuuchi Y, Benetatos CA, Condon SM, Wong WWL, Silke J, Vaux DL, Vince JE, RIPK3 promotes cell death and NLRP3 inflammasome activation in the absence of MLKL. Nat. Commun 6 (2015), doi:10.1038/ncomms7282.
47. Frank D, Vince JE, Pyroptosis versus necroptosis: similarities, differences, and crosstalk. Cell Death Differ. 26, 99–114 (2019). [PubMed: 30341423]
48. Lin Y, Yu M, Fan T, Insights into mechanisms of pranoprofen-induced apoptosis and necroptosis in human corneal stromal cells. 320, 9–18 (2020).
49. Su W, Zhao J, Fan T, Dose- and Time-Dependent Cytotoxicity of Carteolol in Corneal Endothelial Cells and the Underlying Mechanisms. 11, 1–14 (2020).
50. You X, Fan T, Jiang G, Phenylephrine induces necroptosis and apoptosis in corneal epithelial cells dose- and time-dependently. 428, 2–10 (2019).
51. Yerramothu P, Vijay AK, Willcox MDP, Inflammasomes, the eye and anti-inflammasome therapy. Eye. 32, 491–505 (2018). [PubMed: 29171506]
52. Zheng Q, Ren Y, Reinach PS, She Y, Xiao B, Hua S, Qu J, Chen W, Reactive oxygen species activated NLRP3 inflammasomes prime environment-induced murine dry eye. Exp. Eye Res 125, 1–8 (2014). [PubMed: 24836981]
53. Niu L, Zhang S, Wu J, Chen L, Wang Y, Upregulation of NLRP3 inflammasome in the tears and ocular surface of dry eye patients. PLoS One. 10, 1–13 (2015).
54. Kaneko M, Imaizumi K, Saito A, Kanemoto S, Asada R, Matsuhisa K, Ohtake Y, ER Stress and Disease: Toward Prevention and Treatment. Biol. Pharm. Bull 40, 1337–1343 (2017). [PubMed: 28867719]
55. Tawiah A, Cornick S, Moreau F, Gorman H, Kumar M, Tiwari S, Chadee K, High MUC2 Mucin Expression and Misfolding Induce Cellular Stress, Reactive Oxygen Production, and Apoptosis in Goblet Cells. Am. J. Pathol 188, 1354–1373 (2018). [PubMed: 29545196]

56. Burman A, Tanjore H, Blackwell TS, Endoplasmic reticulum stress in pulmonary fibrosis. Matrix Biol. 68–69, 355–365 (2018).
57. Pathinayake PS, Hsu ACY, Waters DW, Hansbro PM, Wood LG, Wark PAB, Understanding the Unfolded Protein Response in the Pathogenesis of Asthma. Front. Immunol 9, 1–13 (2018). [PubMed: 29403488]
58. Barabutis N, Unfolded Protein Response supports endothelial barrier function. Biochimie. 165, 206–209 (2019). [PubMed: 31404589]
59. Vladykovskaya E, Sithu SD, Haberzettl P, Wickramasinghe NS, Merchant ML, Hill BG, McCracken J, Agarwal A, Dougherty S, Gordon SA, Schuschke DA, Barski OA, O'Toole T, D'Souza SE, Bhatnagar A, Srivastava S, Lipid Peroxidation Product 4-Hydroxy- trans −2-nonenal Causes Endothelial Activation by Inducing Endoplasmic Reticulum Stress. J. Biol. Chem 287, 11398–11409 (2012). [PubMed: 22228760]
60. Iurlaro R, Muñoz-Pinedo C, Cell death induced by endoplasmic reticulum stress. FEBS J. 283, 2640–2652 (2016). [PubMed: 26587781]
61. Saveljeva S, Mc Laughlin SL, Vandenabeele P, Samali A, Bertrand MJM, Endoplasmic reticulum stress induces ligand-independent TNfR1-mediated necroptosis in L929 cells. Cell Death Dis. 6, e1587–10 (2015). [PubMed: 25569104]
62. Castro I, Albornoz N, Aguilera S, Barrera M-J, González S, Núñez M, Carvajal P, Jara D, Lagos C, Molina C, Urzúa U, Hermoso MA, González M-J, Aberrant MUC1 accumulation in salivary glands of Sjögren's syndrome patients is reversed by TUDCA in vitro. Rheumatology. 59, 742–753 (2020). [PubMed: 31377809]
63. Seo Y, Ji YW, Lee SM, Shim J, Noh H, Yeo A, Park C, Park MS, Chang EJ, Lee HK, Activation of HIF-1α (hypoxia inducible factor-1α) prevents dry eye-induced acinar cell death in the lacrimal gland. Cell Death Dis. 5, 1–10 (2014).
64. Coursey TG, Tukler Henriksson J, Barbosa FL, De Paiva CS, Pflugfelder SC, Interferon-γ-Induced Unfolded Protein Response in Conjunctival Goblet Cells as a Cause of Mucin Deficiency in Sjögren Syndrome. Am. J. Pathol 186, 1547–1558 (2016). [PubMed: 27085137]
65. Cho BJ, Hwang JS, Shin YJ, Kim JW, Chung TY, Hyon Y, Rapamycin rescues endoplasmic reticulum stress–induced dry eye syndrome in mice. Investig. Ophthalmol. Vis. Sci 60, 1254–1264 (2019). [PubMed: 30924850]
66. Woodward AM, Di Zazzo A, Bonini S, Argüeso P, Endoplasmic reticulum stress promotes inflammation-mediated proteolytic activity at the ocular surface. Sci. Rep 10, 1–9 (2020). [PubMed: 31913322]
67. Lee Y, Kim MT, Rhodes G, Sack K, Son SJ, Rich CB, Kolachalama VB, Gabel CV, Trinkaus-Randall V, Sustained Ca 2+ mobilizations: A quantitative approach to predict their importance in cell-cell communication and wound healing. PLoS One. 14, 1–22 (2019).
68. Minns MS, Teicher G, Rich CB, Trinkaus-Randall V, Purinoreceptor P2X7 regulation of Ca2+ mobilization and cytoskeletal rearrangement is required for corneal reepithelialization after injury. Am. J. Pathol 186, 285–296 (2016). [PubMed: 26683661]
69. Byun YS, Yoo YS, Kwon JY, Joo JS, Lim SA, Whang WJ, Mok JW, Choi JS, Joo CK, Diquafosol promotes corneal epithelial healing via intracellular calcium-mediated ERK activation. Exp. Eye Res (2016), doi:10.1016/j.exer.2015.10.013.
70. Leiper LJ, Walczysko P, Kucerova R, Ou J, Shanley LJ, Lawson D, V Forrester J, McCaig CD, Zhao M, Collinson JM, The roles of calcium signaling and ERK1/2 phosphorylation in a Pax6+/− mouse model of epithelial wound-healing delay. BMC Biol. 4, 27(2006). [PubMed: 16914058]
71. Edwards BS, Dang AK, Murtazina DA, Dozier MG, Whitesell JD, Khan SA, Cherrington BD, Amberg GC, Clay CM, Navratil AM, Dynamin is required for GnRH signaling to L-type calcium channels and activation of ERK. Endocrinology. 157, 831–843 (2016). [PubMed: 26696122]
72. Li J, Yan B, Si H, Peng X, Zhang SL, Hu J, Atlastin regulates store-operated calcium entry for nerve growth factor-induced neurite outgrowth. Sci. Rep 7, 1–9 (2017). [PubMed: 28127051]
73. Muriel MP, Dauphin A, Namekawa M, Gervais A, Brice A, Ruberg M, Atlastin-1, the dynamin-like GTPase responsible for spastic paraplegia SPG3A, remodels lipid membranes and may form tubules and vesicles in the endoplasmic reticulum. J. Neurochem 110, 1607–1616 (2009). [PubMed: 19573020]

74. Naon D, Zaninello M, Giacomello M, Varanita T, Grespi F, Lakshminaranayan S, Serafini A, Semenzato M, Herkenne S, Hernández-Alvarez MI, Zorzano A, De Stefani D, Dorn GW, Scorrano L, Critical reappraisal confirms that Mitofusin 2 is an endoplasmic reticulum-mitochondria tether. Proc. Natl. Acad. Sci. U. S. A 113, 11249–11254 (2016). [PubMed: 27647893]

75. De Brito OM, Scorrano L, Mitofusin 2 tethers endoplasmic reticulum to mitochondria. Nature. 456, 605–610 (2008). [PubMed: 19052620]

76. Giorgi C, Marchi S, Pinton P, The machineries, regulation and cellular functions of mitochondrial calcium. Nat. Rev. Mol. Cell Biol 19, 713–730 (2018). [PubMed: 30143745]

77. Hayashi T, Su TP, Sigma-1 Receptor Chaperones at the ER- Mitochondrion Interface Regulate Ca2+ Signaling and Cell Survival. Cell. 131, 596–610 (2007). [PubMed: 17981125]

78. Gipson IK, Spurr-Michaud S, Argüeso P, Tisdale A, Ng TF, Russo CL, Mucin gene expression in immortalized human corneal-limbal and conjunctival epithelial cell lines. Invest. Ophthalmol. Vis. Sci 44, 2496–506 (2003). [PubMed: 12766048]

79. Argüeso P, Guzman-Aranguez A, Mantelli F, Cao Z, Ricciuto J, Panjwani N, Association of cell surface mucins with galectin-3 contributes to the ocular surface epithelial barrier. J. Biol. Chem (2009), doi:10.1074/jbc.M109.033332.

80. McDermott AM, Baidouri H, Woodward AM, Kam WR, Liu Y, Chen X, Ziemanski JF, Vistisen K, Hazlett LD, Nichols KK, Argüeso P, Sullivan DA, Short Tandem Repeat (STR) Profiles of Commonly Used Human Ocular Surface Cell Lines. Curr. Eye Res (2018), doi:10.1080/02713683.2018.1480043.

81. Argüeso P, Tisdale A, Spurr-Michaud S, Sumiyoshi M, Gipson IK, Mucin characteristics of human corneal-limbal epithelial cells that exclude the rose bengal anionic dye. Investig. Ophthalmol. Vis. Sci 47, 113–119 (2006). [PubMed: 16384952]

82. Petronilli V, Miotto G, Canton M, Colonna R, Bernardi P, Di Lisa F, Imaging the mitochondrial permeability transition pore in intact cells. BioFactors. 8, 263–272 (1998). [PubMed: 9914828]

83. Strober W, Curr. Protoc. Immunol, in press, doi:10.1002/0471142735.ima03bs111.

Highlights

- The wet mucosal epithelia of the ocular surface protect against threats to the eye
- Dynasore is a cell-permeable, small molecule inhibitor of dynamin GTPases
- Dynasore was shown to protect the mucosal epithelia against oxidative stress
- In a novel mechanism, dynasore is now shown to act by maintaining Ca^{+2} homeostasis
- Dynasore thereby inhibits the PERK branch of the unfolded protein response

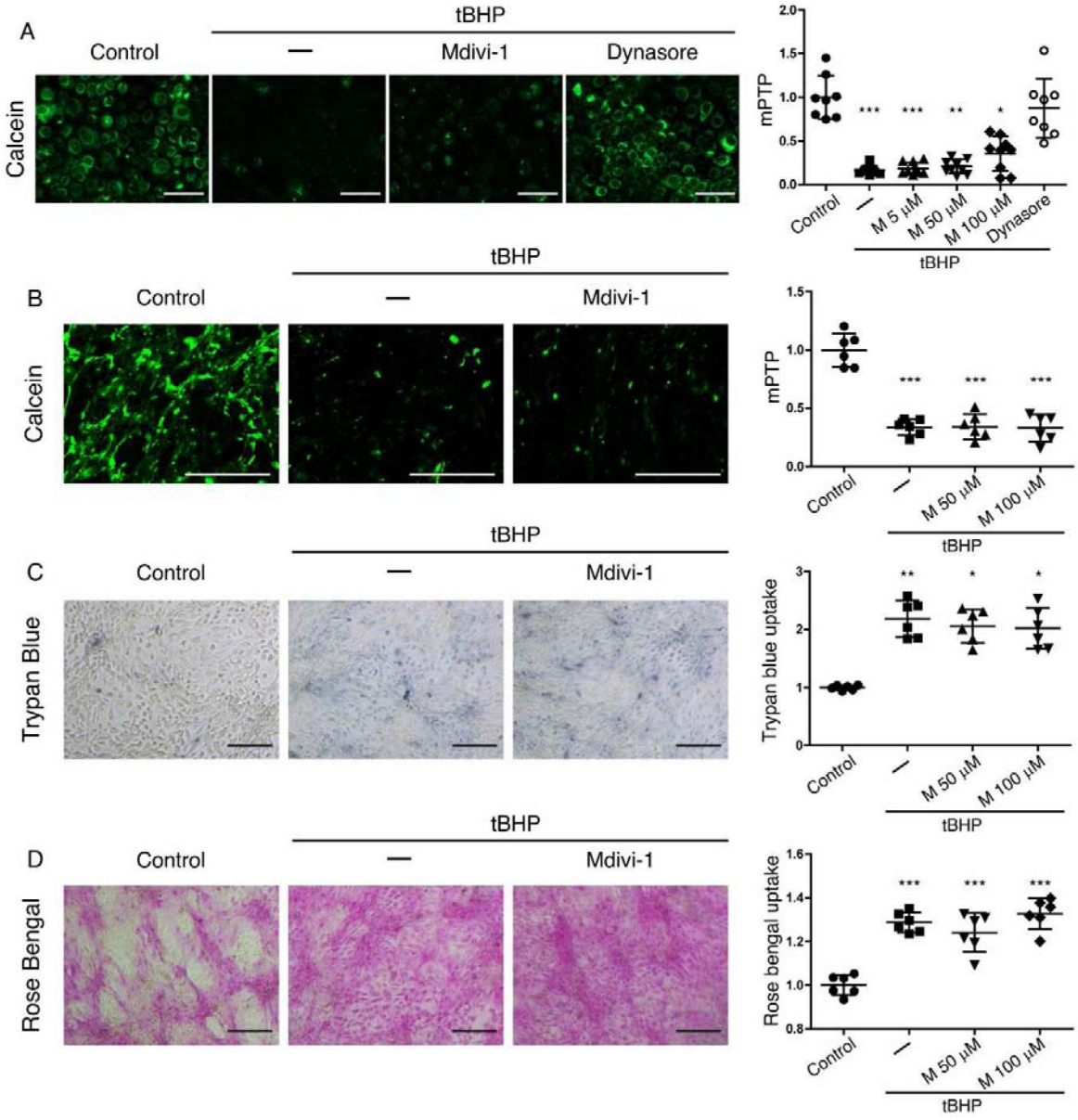

Figure 1. Dynasore, but not DRP1 inhibitor mdivi-1, protects mitochondria and transcellular barriers in HCLE cells subjected to oxidative stress.

(A) Representative images and fluorescence quantification for the analysis of mPTP opening with the calcein-AM/$CoCl_2$ assay in monolayer cultures of HCLE cells exposed to tBHP (1 mM) for 2 hrs while being treated with mdivi-1 (5, 50 and 100 μM), dynasore (40 μM), or DMSO vehicle (–). Unstressed cells kept in growth medium with the same DMSO concentration served as control. $n = 3$

(B-D) Stratified cultures of HCLE cells with mucosal differentiation were exposed to tBHP (10 mM) while being treated with mdivi-1 (50 and 100 μM) or DMSO vehicle (–). Unstressed cells kept in growth medium with the same DMSO concentration served as control.

(B) Representative images and quantification of mPTP opening, with the calcein-AM/$CoCl_2$ assay ($n = 2$)
(C) plasma membrane transcellular barrier integrity with trypan blue exclusion ($n = 2$)
(D) and mucosal transcellular barrier integrity with rose bengal exclusion ($n = 2$)
The data are presented as mean ± standard deviation. Significant differences were determined using the Kruskal-Wallis test with Dunn's post-hoc test (A and C) or ANOVA with Bonferroni's post-hoc test (B and D), after determining the homogeneity of the variances with the Bartlett's test. * P<0.05; *** P<0.001. Scale bar: 100 μm (**A**); 1 mm (**B**); 200 μm (**C, D**).

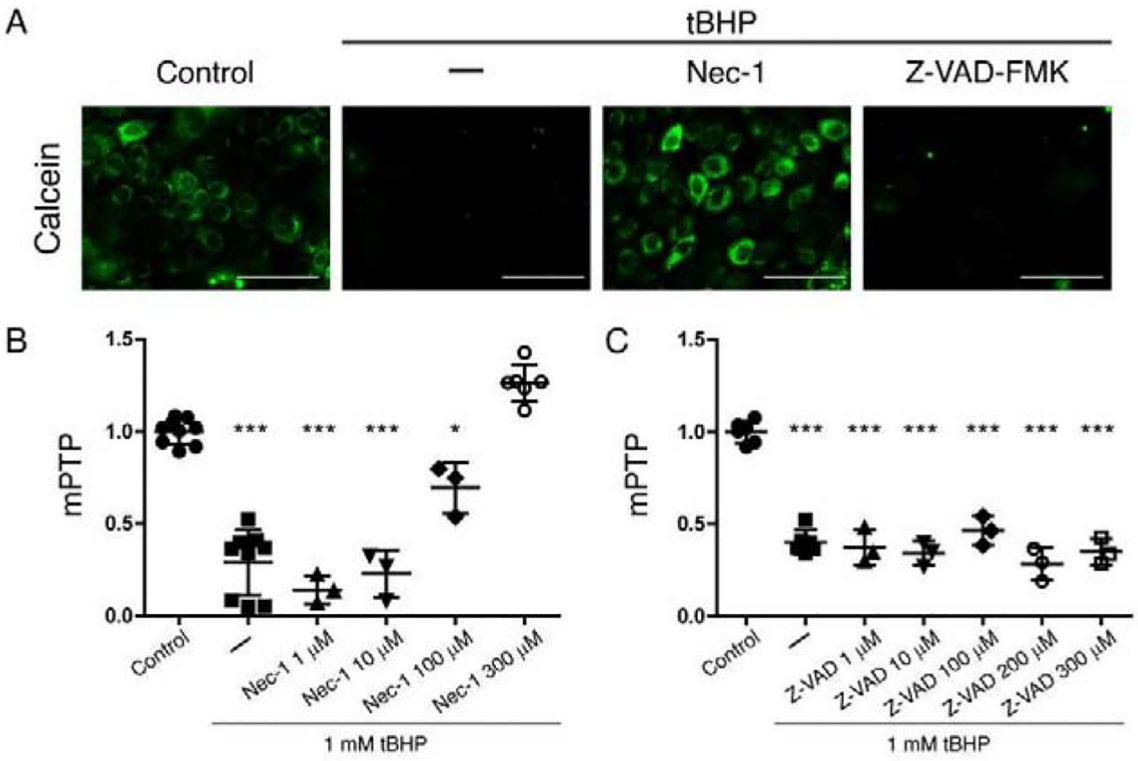

Figure 2. RIPK1 inhibitor necrostatin-1 and pan-caspase inhibitor Z-VAD-FMK protect mitochondria in HCLE cells subjected to oxidative stress.

Monolayer cultures of HCLE cells were exposed to tBHP (1 mM) for 2 hrs while being treated with different concentrations of necrostatin-1(1 μM to 300 μM), Z-VAD-FM (1 μM to 300 μM), or DMSO vehicle (–). Unstressed cells kept in growth medium with the same DMSO concentration served as control. The calcein-AM/$CoCl_2$ assay was then performed to assess mPTP opening.

(A) Representative images for each treatment.

(B) Quantification of fluorescence intensity for the different necrostatin-1 concentrations (results from 3 independent experiments).

(C) Quantification of fluorescence intensity for the different concentrations of Z-VAD-FMK (results from 2 independent experiments).

The data are presented as mean ± standard deviation. Significant differences were determined using ANOVA with Bonferroni's post-hoc test. * P<0.05; *** P<0.001. Scale bar: 100 μm

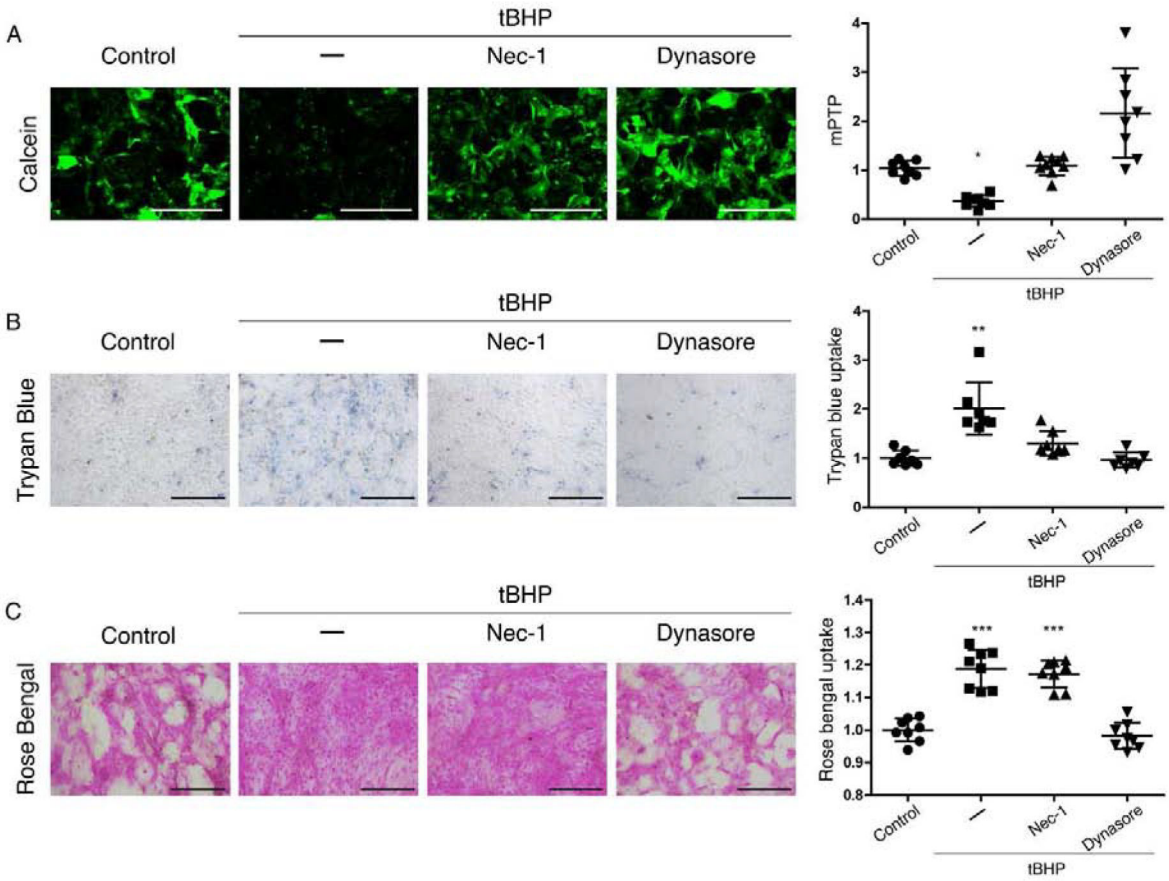

Figure 3. Dynasore and RIPK1 inhibitor necrostatin-1 protect mitochondria and the plasma membrane barrier in HCLE cells subjected to oxidative stress, but only dynasore protects the mucosal barrier

Stratified cultures of HCLE cells with mucosal differentiation were exposed to tBHP (10 mM) for 2 hrs while being treated with either 300 μM necrostatin-1, 80 μM dynasore, or the same amount of DMSO vehicle (–). Unstressed cells kept in growth medium with the same DMSO concentration served as control.

(A) Representative images and quantification of mPTP opening, with the calcein-AM/$CoCl_2$ assay ($n = 3$)

(B) Plasma membrane transcellular barrier integrity with trypan blue exclusion ($n = 3$)

(C) Mucosal transcellular barrier integrity with rose bengal exclusion ($n = 3$)

The data are presented as mean ± standard deviation. Significant differences were determined using the Kruskal-Wallis test with Dunn's post-hoc test (A and B) or ANOVA with Bonferroni's post-hoc test (C), after determining the homogeneity of the variances with the Bartlett's test. * P<0.05; *** P<0.001. Scale bar: 1 mm (**A**); 200 μm (**B, C**).

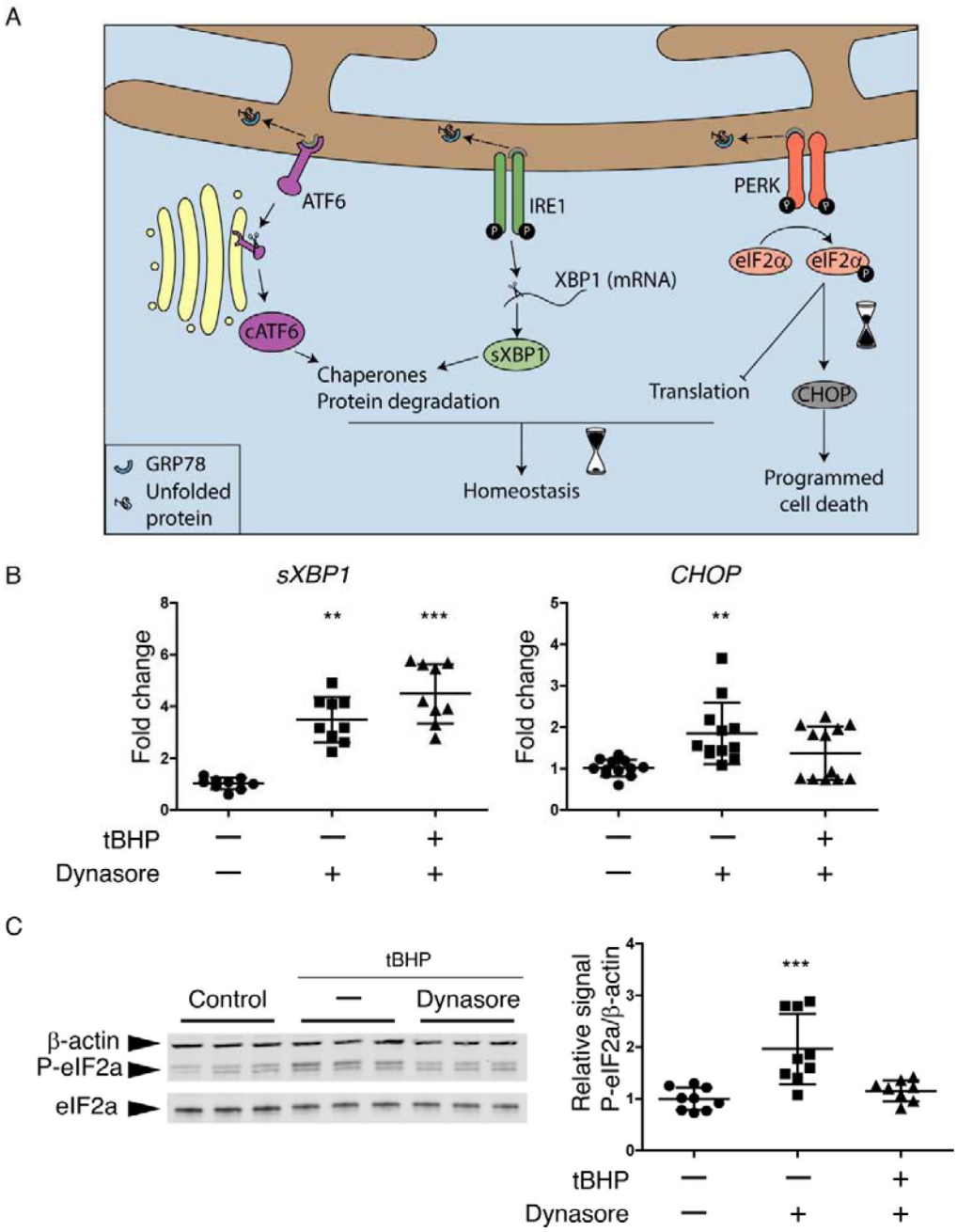

Figure 4. The UPR is activated in HCLE cells subjected to oxidative stress; dynasore inhibits the PERK branch

(A) Schematic of the UPR. Dissociation of GRP78 from ATF6, IRE1 and PERK to bind to accumulated unfolded proteins is usually the start point that activates the UPR. The activation of each one of the sensors (ATF6, IRE1 and PERK) produces a second messenger. They main effects of cATF6 and sXBP1 are to increase chaperones production and the activation of ERAD for protein degradation, which can help to recover the homeostasis. While the phosphorylation of eIF2α can reduce protein translation to maintain homeostasis, it can also increase the expression of *CHOP* when ER stress is prolonged, leading to cell death.

(B and C) Stratified cultures of HCLE cells with mucosal differentiation were exposed to tBHP (10 mM) for 2 hrs while also being treated with 80 μM dynasore or DMSO vehicle. Unstressed cells kept in growth medium with the same DMSO concentration served as control. At the end of the experiment, RNA or protein was isolated.

(B) Relative gene expression of *sXBP1* ($n = 3$) and *CHOP* ($n = 4$) was calculated with the $2^{-\Delta\Delta Ct}$ method, using the levels of *ACTB* expression as housekeeping and the expression in control cells as the calibrator.

(C) Representative images of western blot for P-eIF2α, eIF2α and ACTB and densitometry analysis of P-eIF2α normalized to β-actin levels as a loading control. $n = 3$.

The data are presented as mean ± standard deviation. Significant differences were determined using the Kruskal-Wallis test with Dunn's post-hoc test. ** $P<0.01$; *** $P<0.001$.

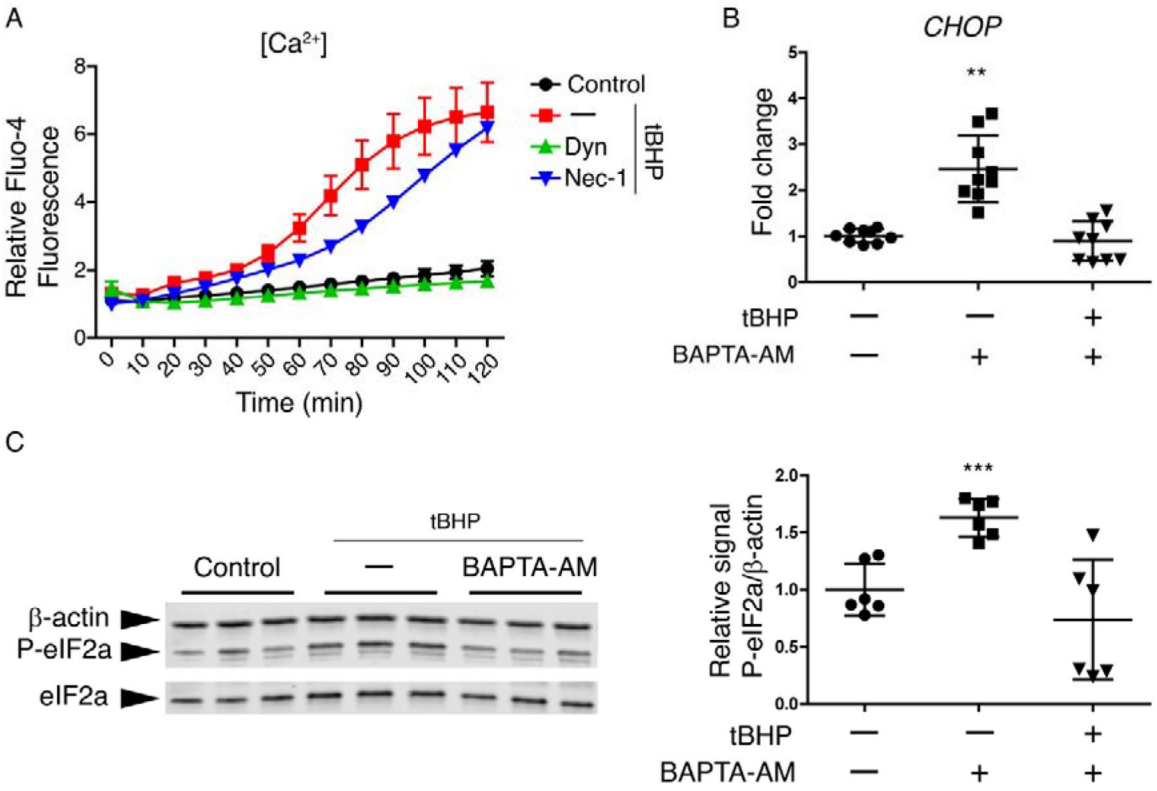

Figure 5. Dynasore inhibits the Ca^{2+} increase induced by oxidative stress, which is enough to reduce the activation of P-eIF2a/CHOP pathway.

(A) Monolayer cultures of HCLE cells were incubated with Fluo-4 Direct™ containing probenecid (2.5 mM). Then cells were exposed to tBHP (1 mM) for 2 hrs while being treated with either dynasore (40 μM), necrostatin-1 (300 μM), or DMSO vehicle (–). Unstressed cells kept in growth medium with the same DMSO concentration served as control. Changes in fluorescence over the times course were monitored under a fluorescence microscope. ($n = 3$)

(B and C) Stratified cultures of HCLE cells with mucosal differentiation were exposed to tBHP (10 mM) for 2 hrs after 1 h of preincubation with either BAPTA-AM (200 μM) or DMSO vehicle (–). Unstressed cells kept in growth medium with the same DMSO concentration served as control. At the end of the experiment, RNA or protein was isolated.

(B) Relative gene expression of *CHOP* was calculated with the $2^{-\Delta\Delta Ct}$ method, using the levels of *β-actin* expression as housekeeping and the expression in control cells as the calibrator. $n = 3$.

(C) Representative images of western blot for P-eIF2α, eIF2α and β-actin and densitometry analysis of P-eIF2α normalized to β-actin levels as a loading control. $n = 2$.

The data are presented as mean ± standard deviation. Significant differences were determined using the Kruskal-Wallis test with Dunn's post-hoc test. * P<0.05; ** P<0.01.

Table 1.

Primer sequences for RT-PCR.

Gene	Primer sequence
sXBPl	Fwd: CTGAGTCCGAATCAGGTGCAG
	Rev: ATCCATGGGGAGATGTTCTGG
CHOP	Fwd: AGAACCAGGAAACGGAAACAGA
	Rev: TCTCCTTCATGCGCTGCTTT
ACTB	Fwd: GTCATTCCAAATATGAGATGCGT
	Rev: GCTATCACCTCCCCTGTGTG